Measurement of cosmic ray electron-positron spectrum with Fermi

Andrea Virtuoso
Università di Trieste
A. A. 2018/2019

Measurement of separate cosmic-ray electron and positron spectra

- Measurement of electron spectrum
- Measurement of positron spectrum
- Positron fraction $e^+/(e^+ + e^-)$ between 20 GeV and 200 GeV
- Confirmation that the fraction rises with energy in the 20-100 GeV range

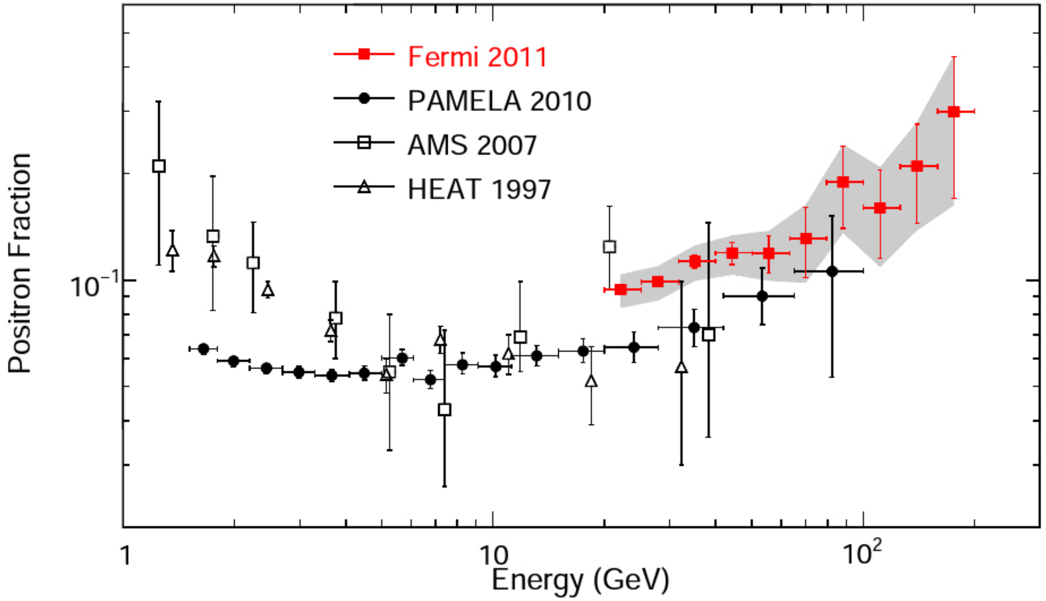

How positrons in CR are produced?

The best established mechanism for producing CR positrons is secondary production: CR nuclei interact inelastically with interstellar gas, producing charged pions that decay to positrons, electrons, and neutrinos. However, this process results in a positron fraction that decreases with energy [4, 17]. The origin of the rising positron fraction at high energy is unknown and has been ascribed to a variety of mechanisms including pulsars, CRs interacting with giant molecular clouds, and dark matter.

Main challenges in e^+ and e^- detection

- How to distinguish between positrons and electrons?
- Effects of Earth's magnetic field (trajectories deflection and consequent east-west effect)
- Necessity to take into account of these effects, but also possibility of using them for distiguish between electrons and positrons

Trajectories deflection

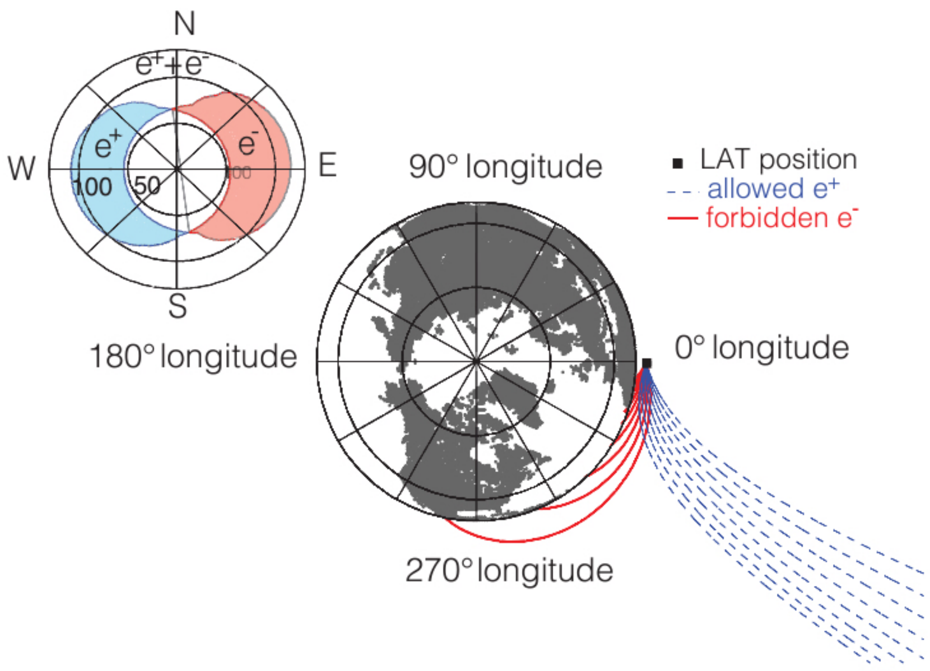

FIG. 1: Examples of calculated electron (red) and positron (blue) trajectories arriving at the detector, for 28 GeV particles arriving within the Equatorial plane (viewed from the North pole). Forbidden trajectories are solid and allowed trajectories are dashed. Inset: the three selection regions (electron-only, positron-only, and both-allowed) for the same particle energy and spacecraft position as the trajectory traces (viewed from the instrument position in the Equatorial plane).

How to take account of Earth's magnetic field effects

- Use of a high precision geomagnetic field model to trace charged particles' trajectories and determine allowed and forbidden regions for positrons and electrons
- To remove atmospheric electron and positrons (deflected by the geomagnetic field)

Background problems

- Necessity to take into account of a background of CR protons and heavier nuclei
- This background is 2-3 orders of magnitude larger than the positron flux
- Application of separation criteria and indipendent methods to estimate the residual proton contamination (fits, Monte Carlo simulations)

Fit of signal + background

- Evaluation of size of showers in the calorimeter (significant difference between electromagnetic showers from hadronic interactions)
- Use of a control region to costrain parameters

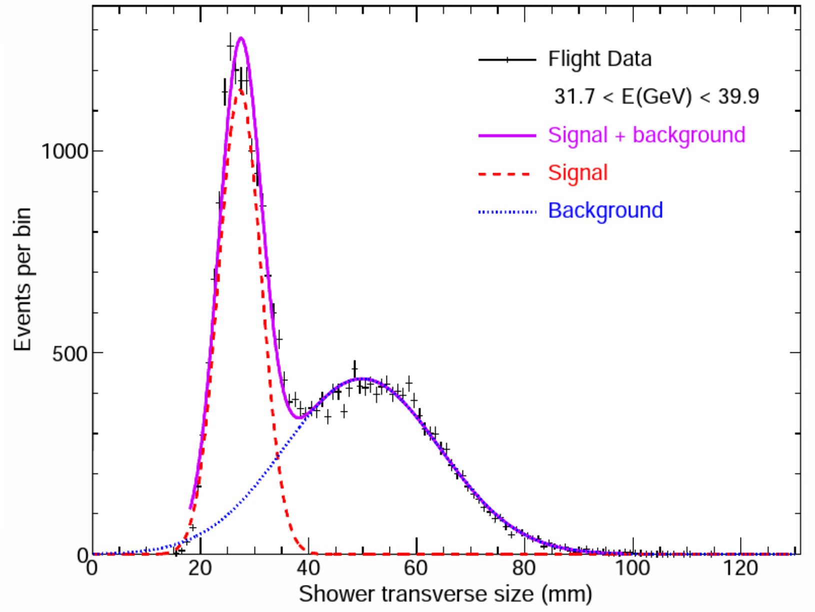

FIG. 3: Transverse shower size distribution in the electron-only region. In the positron-only region, the number of events with small transverse shower size is smaller, but the mean and width of the distribution are similar.

Monte Carlo simulations

- Simulations made with GEANT 4
- Comparison of a variety of distributions between MC and flight data
- The rate of MC protons agree with flight data within about 8%

Results

- 10-16% uncertainty in the positron flux for the fit method, 8-19% for the MC method (depending on energy)
- Spectra are well described by power laws [(2.02±0.22 × 10^{-3} GeV^{-1} m^{-2} s^{-1} sr^{-1})$(E/20GeV)^{-2.77\pm0.14}$ for positron spectrum, (2.07±0.13 × 10^{-2} GeV^{-1} m^{-2} s^{-1} sr^{-1})(E 20GeV)$^{-3.19\pm0.07}$ for electron spectrum]

Results

Energy	$J(e^+) \times 10^5$	$J(e^-) \times 10^4$	$\frac{J(e^+)}{J(e^+)+J(e^-)}$
20.0 – 25.2	$160 \pm 5^{+20}_{-21}$	$154 \pm 1^{+14}_{-14}$	$.094 \pm .003^{+.010}_{-.010}$
25.2 – 31.7	$80.2 \pm 2.9^{+10}_{-10}$	$72.8 \pm .6^{+6.5}_{-6.5}$	$.099 \pm .003^{+.010}_{-.011}$
31.7 – 39.9	$43.4 \pm 2.0^{+4.9}_{-5.1}$	$34.1 \pm .4^{+2.5}_{-2.5}$	$.113 \pm .005^{+.012}_{-.012}$
39.9 – 50.2	$21.8 \pm 1.7^{+2.5}_{-2.6}$	$16.1 \pm .3^{+1.2}_{-1.2}$	$.119 \pm .008^{+.012}_{-.013}$
50.2 – 63.2	$10.7 \pm 1.4^{+1.2}_{-1.3}$	$7.89 \pm .28^{+.58}_{-.58}$	$.119 \pm .014^{+.012}_{-.013}$
63.2 – 79.6	$5.52 \pm 1.4^{+.66}_{-.68}$	$3.66 \pm .23^{+.27}_{-.27}$	$.131 \pm .029^{+.014}_{-.014}$
79.6 – 100	$3.90 \pm 1.2^{+.46}_{-.48}$	$1.67 \pm .21^{+.12}_{-.12}$	$.189 \pm .049^{+.018}_{-.019}$
100 – 126	$1.83 \pm .57^{+.22}_{-.28}$	$.97 \pm .12^{+.08}_{-.08}$	$.160 \pm .045^{+.017}_{-.023}$
126 – 159	$1.28 \pm .45^{+.15}_{-.20}$	$.481 \pm .085^{+.039}_{-.039}$	$.210 \pm .065^{+.021}_{-.030}$
159 – 200	$.911 \pm .48^{+.13}_{-.16}$	$.214 \pm .069^{+.011}_{-.011}$	$.30 \pm .13^{+.03}_{-.04}$

TABLE I: Flux (GeV^{-1} m^{-2} s^{-1} sr^{-1}) and positron fraction as a function of energy (GeV). Uncertainties are ±stat ±sys.

Results

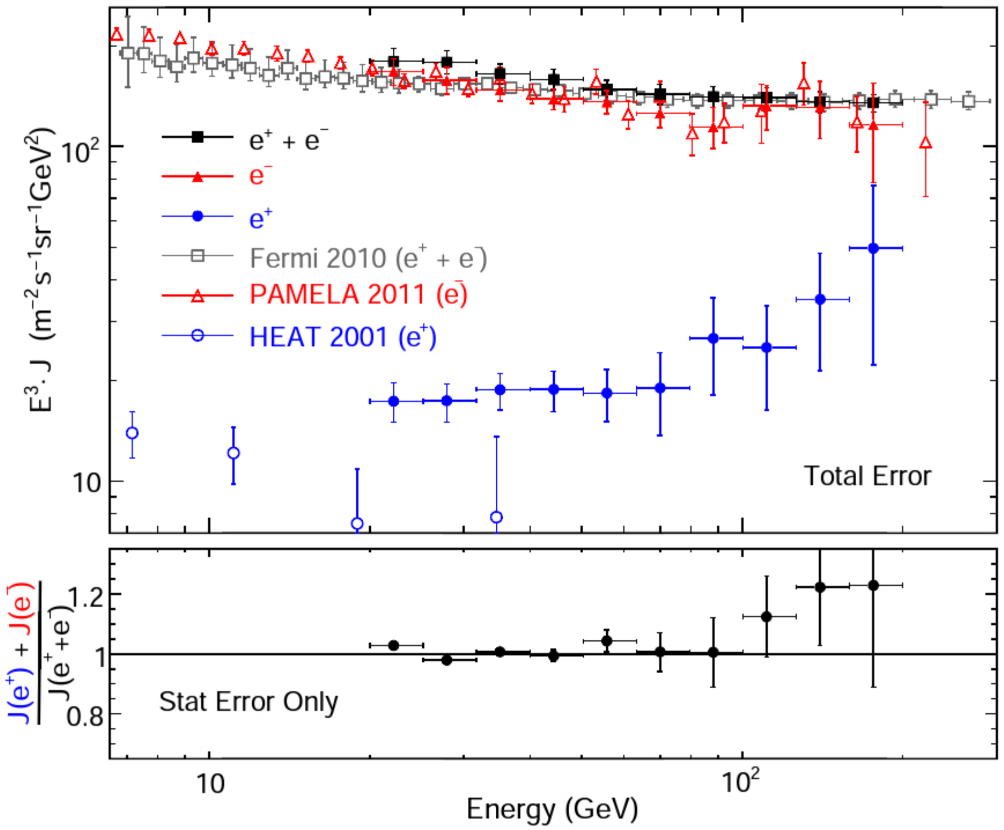

FIG. 4: Energy spectra for e^+, e^-, and $e^+ + e^-$ (control region). In the control region where both species are allowed, this analysis reproduces the Fermi LAT results reported previously for the total electron plus positron spectrum [20, 21] (gray). Previous results form HEAT [9] and PAMELA [38] are shown for reference. The bottom panel shows that the ratio between the sum and the control flux is consistent with 1 as expected.

Results

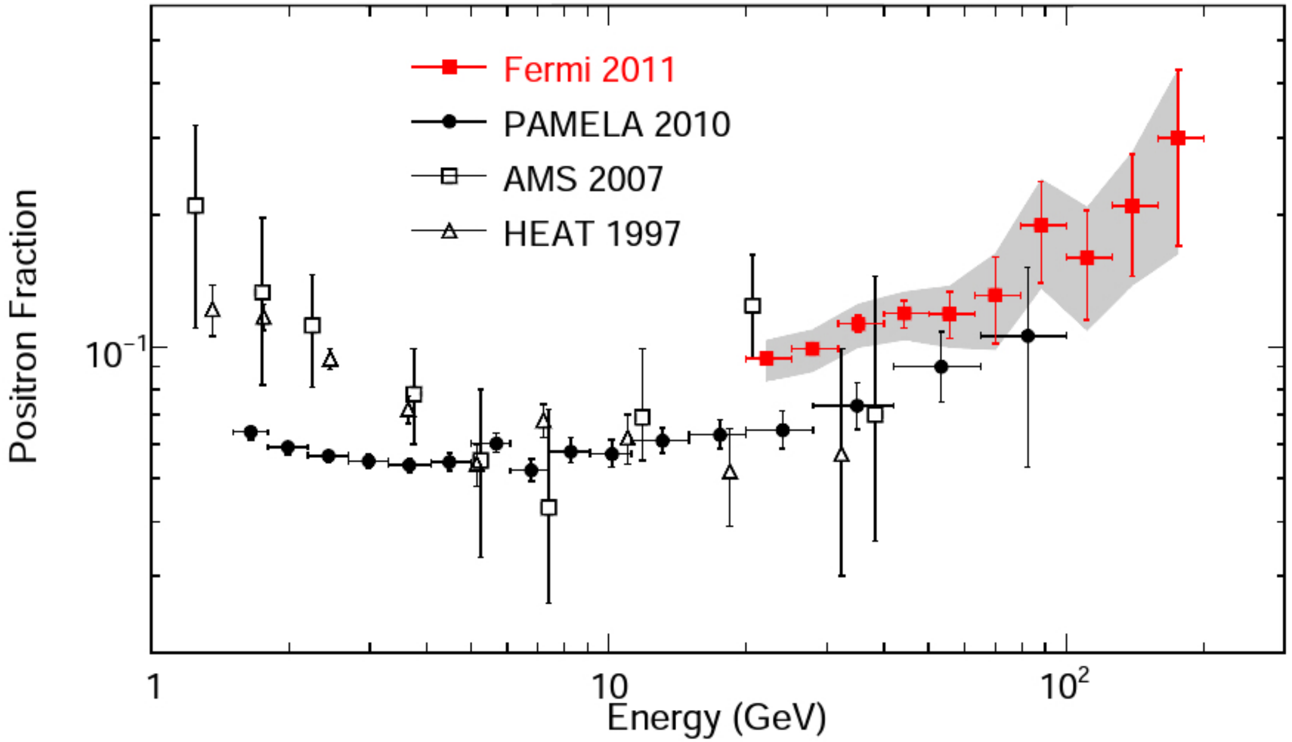

FIG. 5: Positron fraction measured by the Fermi LAT and by other experiments [7, 14, 16]. The Fermi statistical uncertainty is shown with error bars and the total (statistical plus systematic uncertainty) is shown as a shaded band.

Main conclusions of this article

- Confirmation of the previous PAMELA's measurements: the positron fraction increases with energy between 20 and 200 GeV
- Necessity of new measurements with greater sensitivity to distinguish between the many possible explanations of this increasing fraction (pulsars? CR's interaction with giant molecular clouds? dark matter?); note that the positron fraction increasing agrees with the annihilation/decay models for dark matter, see also **arXiv:1008.4646 [astro-ph.HE]**

Cosmic-ray electron + positron spectrum from 7 GeV to 2 TeV with the Fermi Large Area Telescope

- Measurement of the cosmic ray electron+positron (CRE) spectrum between 7 GeV and 2 TeV
- Main results:

1) the spectrum is well fit by a broken power law with a break energy at about 50 GeV
2) above 50 GeV the spectrum is well described by a single power law
3) an exponential cutoff lower than 1.8 TeV is excluded at 95% CL

Event selection

- Two indipendent analysis

1) High energy (HE) analysis (above 42 GeV)
2) Low energy (LE) analysis (between 7 and 70 GeV)

- In both analysis, use of simple cuts for reducing the residual proton contamination
- Necessity to remove photons, alphas and heavier ions contribute
- These cuts are combined with further selections based on multivariate classification analysis done with Boosted Decision Trees (BDT) improved with simulated datasets generated with Monte Carlo

High energy analysis

- Training of BDTs with the same set of variables (one BDT for each bin of energy, for a total amount of 8 bins that span the energies between 31.6 GeV and 3.16 TeV); these discriminating variables characterize the shower trajectory and topology
- Necessity to an agreement between distributions measured in data and predicted by the simulations; the widths of the distributions are in good agreement but for some variables the position of the peak is shifted, so there are needed additive corrections (Individual Variables Calibration, IVC)
- Necessity of others corrections for proton range

High energy analysis

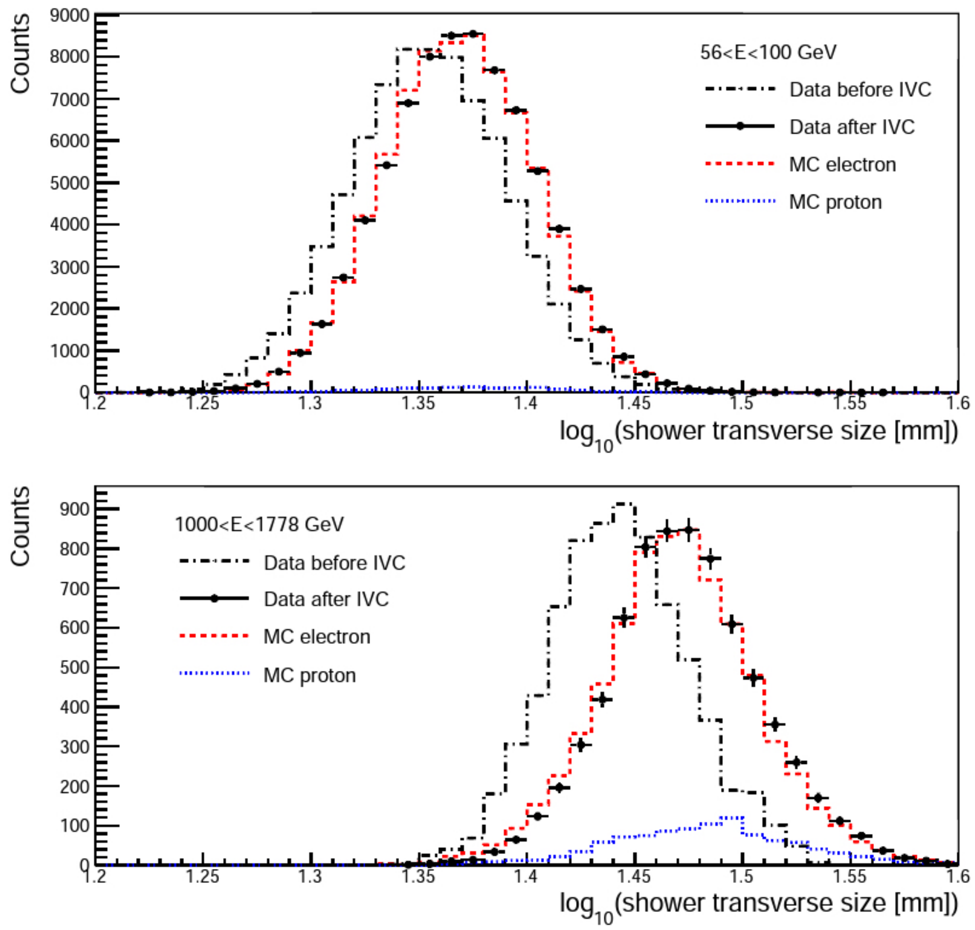

FIG. 2. The logarithm of the shower transverse size before (*black lines*) and after (*black circles*) IVC correction for events between 56 and 100 GeV (top) and between 1 and 1.78 TeV (bottom). The contribution from residual background (blue) has been subtracted from the data distributions. The red histograms correspond to the electron simulation.

High energy analysis

- The selection is improved minimizing in the BDT the flux uncertainty
- The difficulty in background rejection increase in energy
- Stop of the HE analysis when the residual contamination reaches 20%, which occurs at 2 TeV

Low energy analysis

- The LE selection is based on the same multivariate analysis approach as used for the HE selection but training only a BDT
- The LE stops at 70 GeV, there is no need to apply the IVC corrections

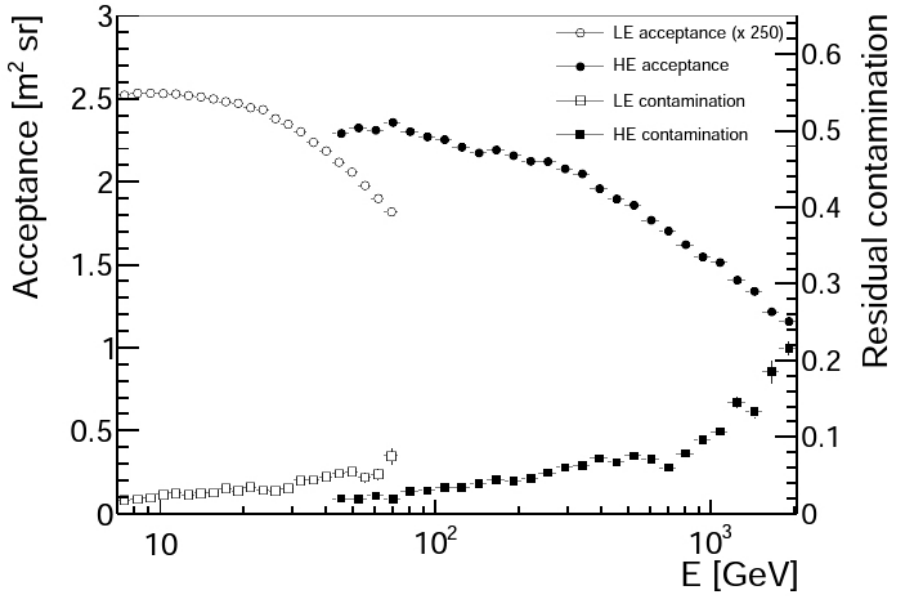

FIG. 6. Acceptance and residual background contamination as a function of energy. The displayed LE acceptance is multiplied by 250 (as if there were no prescale factor due to the on-board filter).

Low energy analysis

- Below about 20 GeV the flux CR is strongly influenced by the Earth‘s magnetic field (dependence on rigidity)
- So there is a fraction of undetected CRE to be estimated evaluating the particle trajectory with simulations
- It’s possible to enhance the effect of the geomagnetic field on CRE’s relevation by a combination of the wide angular aperture of the LAT and its periodic rocking motion with respect to the local zenith: in this way the edge of the field of view is often very close to the Earth. Knowing this some correction factors could be derived

Energy measurement

- The energy reconstruction is performed by fitting the longitudinal shower profile; the fit parameters are the energy and two parameters that describe the shape of the profile: the shape parameter α and the position of the shower maximum T_{max}
- Need to take into account of shower leakage

Energy measurement

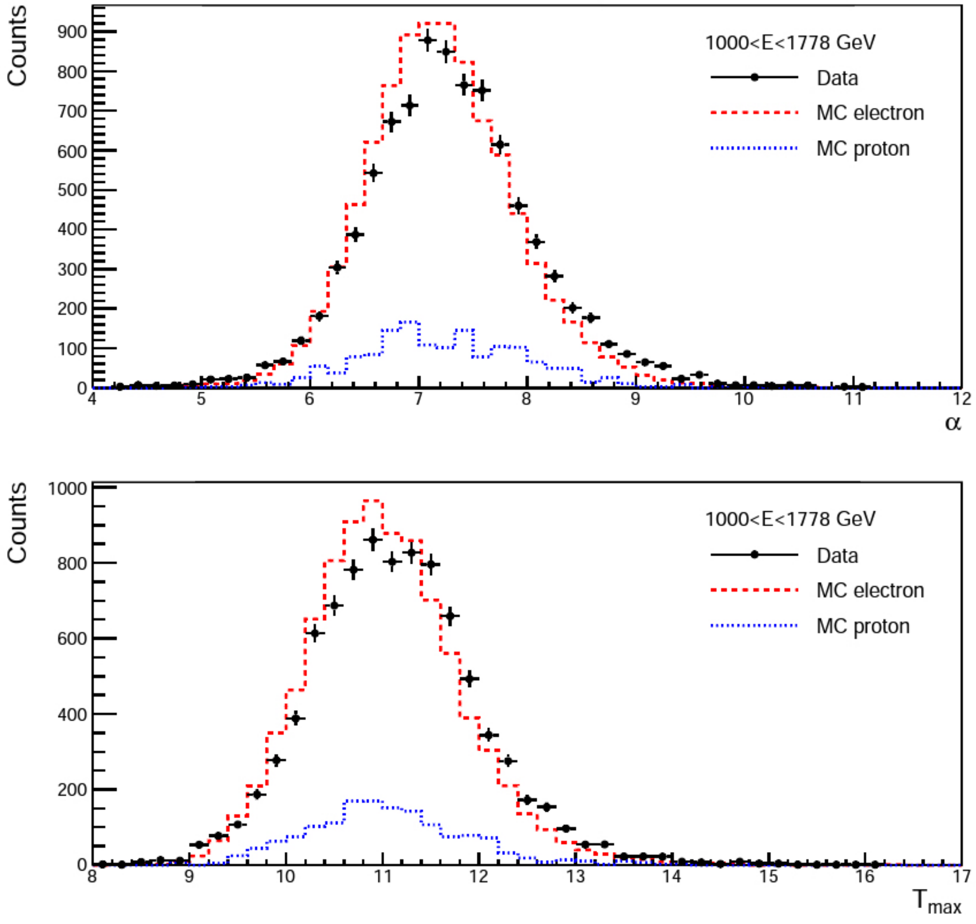

FIG. 11. The shower profile parameters α (top) and $T_{\max}$ (bottom) for events between 1 and 1.78 TeV. The contribution from residual background (blue) has been subtracted from the data distributions. The red histograms correspond to the electron simulation.

Systematic uncertainties

- For HE, need to take into account four sources of systematic uncertainty: three relate to the event selection (acceptance, contamination, IVC), the last one is the uncertainty of the energy measurement
- For LE, need to take into account of acceptance, contamination and the part regarding Earth's geomagnetic field

Results

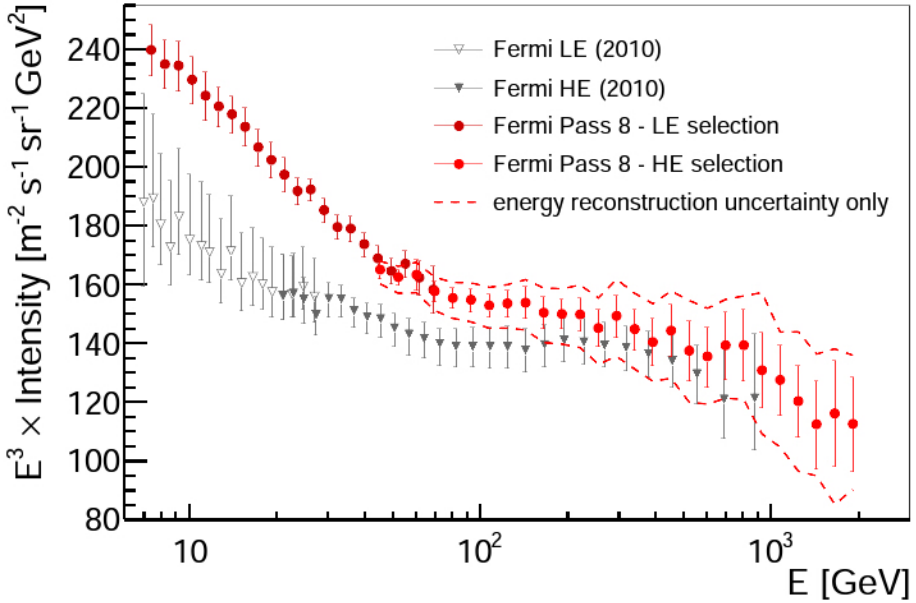

FIG. 13. CRE spectrum between 7 GeV and 2 TeV measured by the LAT and the previous LAT measurement [16]. All error bars represent the quadratic sum of statistical and systematic uncertainties (except the one on the energy measurement). The LAT flux is multiplied by the cube of the representative energy in each bin, computed following Eq. (6) of [33] with an E^{-3} spectrum. The area between the dashed lines corresponds to the uncertainty band due to the LAT energy reconstruction uncertainty only. The 2% systematic uncertainty on the energy scale is not indicated.

Results

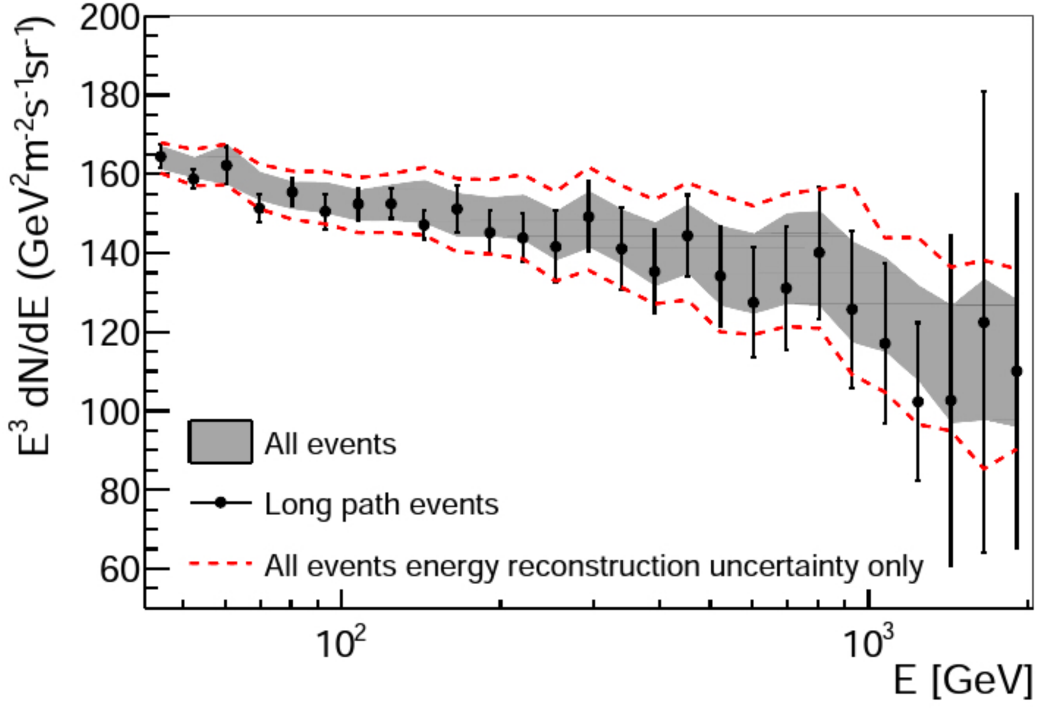

FIG. 14. CRE spectrum between 42 GeV and 2 TeV measured with all events (grey band) and with long-path events (black points). In both cases, the statistical and systematic uncertainties (except for the energy measurement) are added in quadrature. The area between the dashed lines corresponds to the uncertainty band due to the LAT energy reconstruction uncertainty only of the all-event selection.

Results

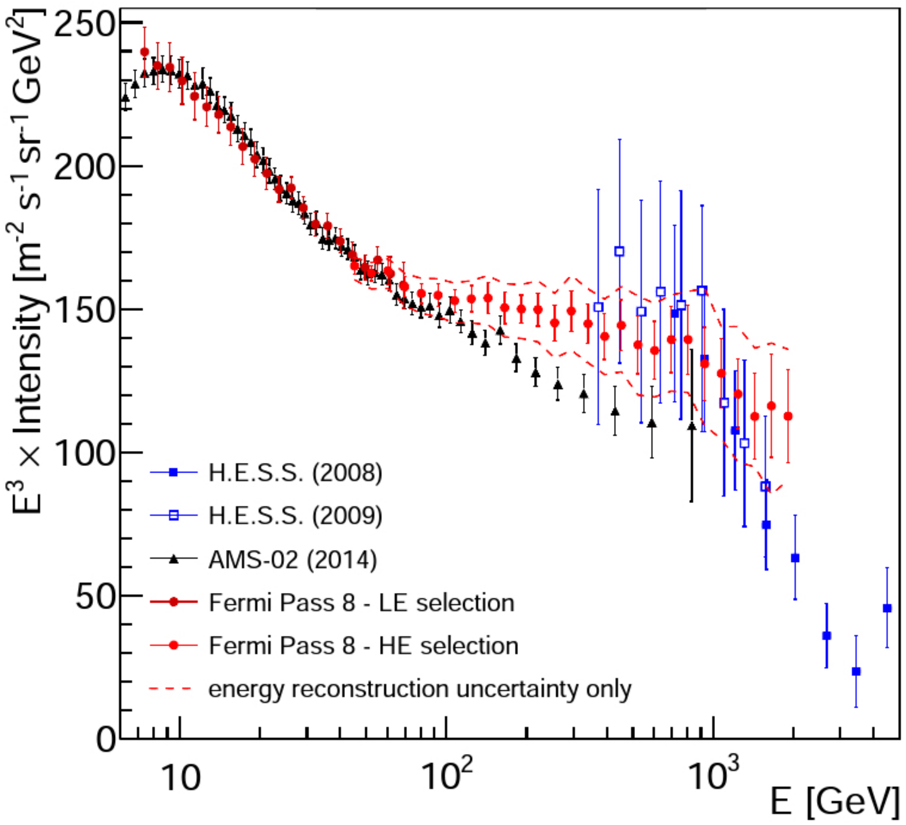

FIG. 15. CRE spectrum between 7 GeV and 2 TeV measured by the LAT along with other recent measurements by AMS-02 [15] and H.E.S.S. [17, 18]. All error bars represent the quadratic sum of statistical and systematic uncertainties (except the one on the energy measurement). The LAT flux is multiplied by the cube of the representative energy in each bin, computed following Eq. (6) of [33] with an E^{-3} spectrum. The area between the dashed lines corresponds to the uncertainty band due to the LAT energy measurement uncertainty only. The 2% systematic uncertainty on the energy scale is not indicated.

Results

- Data suggests the presence of a break in the spectrum
- The break energy is 53 ± 8 GeV and the spectral indices below and above the break are 3.21 ± 0.02 and 3.07 ± 0.02, respectively.
- Exclusion of a cutoff at energies lower than 1.8 TeV at 95 % CL

Thank you for your attention